



The International Society of Precision Agriculture presents the

15th International Conference on Precision Agriculture

26–29 JUNE 2022

Minneapolis Marriott City Center | Minneapolis, Minnesota USA

A low-tech solution to manage within field variability – toward a territorial scale application

Lenoir A^{1,2}., Vandoorne B²., Siah A²., Dumont B¹

¹Université de Liège, Gembloux Agro-Bio Tech, UMRt 1158 BioEcoAgro, Gembloux, Belgique

²JUNIA-ISA, UMRt 1158 BioEcoAgro, Lille, France

A paper from the Proceedings of the
15th International Conference on Precision Agriculture
June 26-29, 2022
Minneapolis, Minnesota, United States

Abstract.

Precision Agriculture is promising to address N management issues in Western Europe. Limited adoption of agricultural technology reveals needs of reliable methods valuing information provided by sensors. This study aims to calibrate a management zone delineation method, originally developed on yield maps, using a vegetation index. This delineation method differentiates high and stable (HS), low and stable (LS) and unstable (U) zones according to spatial and temporal trends within the field. Different steps led to identify the index and a sensing window that best retrieve yield subfield distribution. NDVI was found to be an interesting candidate when sensed during wheat flowering stage. Index-based delineation was then compared to the original delineation from yield maps on six fields. Stable zones (high and low) were well predicted (sensitivity of 0.69 and 0.60) but U zones were not detected with the NDVI-based approach. On the six fields, U zones were originally reduced. We adapted the threshold differentiating HS from LS zones to fit the shape of NDVI distribution. Balance between HS and LS sensibilities improved (respectively 0.67 and 0.68) as well as global accuracy (0.66) of management zones prediction. These findings reveal a good potential to deploy NDVI-based delineation at the scale of a whole territory, which is the next step of this study.

Keywords.

Nitrogen management, delineation method, management zones, vegetation index

Context

European crop production is highly dependent on exogenous nitrogen (N) supplies to increase or even maintain yield levels (Sutton et al. 2011). Many studies have highlighted the economic and environmental consequences of N overuse (Fowler et al. 2013; Galloway et al. 2003; Lécuyer et al. 2014). For decades, scientific and technical efforts have been devoted to develop N fertilization methods that maximize Nitrogen Use Efficiency (NUE). In Belgium and France, the most common approaches consist in balancing annually the difference between soil N supply and crop N demand with mineral N fertilization (Meynard et al. 1997; Nysten et al. 2022; Ravier et al. 2016). Despite substantial improvement in NUE along the past decades, losses of N to the environment are still significant (Billen et al. 2013). Scientific knowledge combined with recent technological development in agriculture, which still requires to be fully adopted by farmers, are offering new opportunities to improve nitrogen management at the sub-field scale.

Hauts-de-France (FR) and Wallonia (BE), the two territories where this study is conducted, gather positives conditions of success to develop precision agriculture approaches. Pierpaoli et al. (2013) identified different key adoption factors of agricultural technologies (e.g., productive potential, size of farms) that correspond to both territories' features (Agreste 2020; SPW 2022). These factors haven't impulse yet a dynamic of technology adoption in Western-Europe (Barnes et al. 2019, Lachia et al. 2020). Beyond economical and structural brakes of adoption, low adoption can be explained by necessary "ease of use" and "usefulness" of technologies. These criteria reveal need of methods to effectively use technologies and transform information they provide into robust diagnostic and decision as confirmed by Lachia et al. (2020). It also reveals the necessity for farmers to be able to perceive technologies interest and get access to it with limited investments (Pierapoli et al. 2013, Barnes et al. 2019).

Satellite images can deliver high precision information on a large scale. Sentinel-2 missions launched by European Space Agency, provide freely available images embedding useful wavelengths for agricultural applications (Delloye et al. 2018). Estimation of yield through remote sensing have historically support different purposes such as N management (Marti et al. 2006; Raun et al. 2001).

The use of freely available satellite images embedded in agronomic methods could be considered as a low-tech solution to support N management and favor adoption by farmers (Bonjean et al. 2022; Rose & Chilvers 2018). Tough, sensing data must be processed and integrated into agronomic methods to be accessible and to provide robust information. In this regard, different Vegetation Indices (VI) have been developed to estimate plant traits such as Leaf Area Index (LAI) or chlorophyll content (Ollinger et al. 2011). At the canopy level, estimated LAI is often used as a proxy of total biomass or final grain yield (Fang et al. 2019, Revill et al. 2019). However, these relationships could be disturbed by external factors such as atmospheric conditions, soil brightness, chlorophyll content variations when the type of relationship depends on plant species (Fang et al. 2019). Therefore, different VIs have been designed to counteract those external influences (Haboudane et al. 2004). Moreover, evolution of plant traits is more or less correlated with final yield according to state of maturity of the crop and the different factors affecting them along the growing period (Marti et al. 2006). These different issues draw up a roadmap to identify (1) the best vegetation index, adapted to targeted species and objectives and (2) the optimal sensing window to retrieve subfield spatial heterogeneity of crop yield and related limiting factors.

Yield has been included in different approaches to characterize within-field heterogeneity as it results from the interaction of several limiting factors and is directly linked to NUE (Hawkesford & Riche 2020). Early studies searched for yield map pre-processing methods to optimally catch within-field patterns and the link between soil and crop variability (Birell et al. 1996; Mulla & Khosla; Raun et al. 2001). However, spatial yield patterns evolve over time making single yield map an ineffective tool to derive agronomic practices (Khosla et al. 2010). An interesting method, developed by Blackmore (2000), delineates management zones, within the field, from yield maps

time-series. This approach integrates both spatial and temporal yield variations. Thus, management zones are defined by the degree of yield stability and of yield level. Three types of zones are identified, the unstable (U) where yield variations are strong over time, the low and stable (LS) and the high and stable (HS) zones. In the later, yield is steadily under or above annual mean yield. This method has been used in different research contexts. Recently, over US Midwest, the method supported the assessment of N fertilization efficiency, revealing large potential of improvement (Basso et al. 2019).

Provided it would be adapted to the agronomic context of west-Europe, Blackmore's method could help further understand and identify the limiting factors of NUE. Indeed, combination of spatial and temporal trends is lacking most of the time in actual N fertilization methods. Managing N with an explicit consideration of spatio-temporal variations (Basso et al., 2007; Blackmore 2000), in combination with recent knowledges on N nutrition dynamic (Lemaire et al. 2008; Ravier et al. 2016), would contribute to create a new framework of N management, adapted to each type of management zone.

The aim of this study is to calibrate Blackmore's methodology to be used with Sentinel-2 data. The study is conducted on different farms of the two territories of Hauts-de-France (FR) and Wallonia (BE) and rely on yield maps obtained. The calibration process was divided in two parts. A first step focuses on the annual relationship existing between spatial crop yield distribution and different vegetation indices computed from images sensed over the crop growing period. In this step, our goal was to identify one vegetation index that best retrieve spatial yield pattern and to define an optimal sensing window to catch yield variability. The second step of the calibration is a validation step. Delineation computed with optimal vegetation index on a selected sensing period was compared, site by site, to Blackmore's delineation calculated with yield maps.

Materials and methods:

Study area

The study is performed on three farms in Wallonia (BE) and Hauts-de-France (FR) from 2016 to 2021. Agronomic and weather contexts are similar with a majority of silty soils (table 1). Crop rotations involve a majority of cereals. Wheat and barley are the most cultivated crops, but rapeseed, potatoes and sugar beet are also well present in the regional soles (Agreste, 2020; SPW, 2022). Soils are characterized by their high silk content and relatively high depth as summarized in table 1 (Dumont et al. 2015).

Table 1 : Study sites features

	Site A	Site B	Site C
Localization	Wallonia	Hauts-de-France	Hauts-de-France
Soil type¹	Stagnic albe-luvisol	Calcosol	Fluvisol
Texture²	Loam	Clay-loam	Silt-loam
Soil depth³	>125 cm	40 [25-85] cm	>100 cm
Mean annual precipitations (mm)⁴	789	680	740
Mean annual temperature (°C)³	10.3	11.1	11.3
Altitude (m)	300	130	25
Number of fields	15	3	17
Average surface (ha)	5.9	9.8	9.7

Yield map data collection and preprocessing

Yield maps were obtained from different harvest combine systems on 35 fields that represent 312 ha (table 1). Fields were selected when uniform N supply is applied every year, thus N is considered as a uniform limiting factor at the sub-field scale.

When raw data was accessible, a two-step process was performed to remove outliers. The first step, considered as global outlier treatment, follows a method developed by Lyle et al. (2014). Yield monitor uses the grain flow and machine speed to estimate grain yield. Values corresponding to cutting width lower than maximum were removed. Distance between records was filtered to keep values within first and last percentile. A last global filtering was applied on yield distribution to keep values within the 90 percent interval of prefiltered values. The second step, the local outlier treatment, used algorithm developed by Leroux et al. (2018). The algorithm was download from Leroux (2020) and few adaptations were applied to include an anisotropic treatment of data, as suggested in this study (Leroux et al. 2018). Results of outlier treatment on yield maps features are summarized in table 2. Spatial yield variations decreased as extremes yields were removed from the different maps. Mean yield increases due to removal of null yield values. Negative skewness decreases and distributions globally bonded to normal distribution. The spatial trend also evolved to reveal a closer spatial structure of the data set. This treatment is consistent with findings of Toscano et al. 2019 who removed approximately 25% of raw yield map values through filtering. Maps from “Site C” (Table 1) were already pre-processed and raw data wasn't accessible.

¹ GIS SOL 2019; Dumont et al. 2015

² Legrain & Block 2009

³ Le Bas 2021

⁴ Météo-France, IRM 2021

Table 2. Distribution and spatial features of yield maps before and after outliers' treatment

	Yield performances					Spatial trends of yield	
	Removed records	Yield range (t.ha ⁻¹)	Mean yield (t.ha ⁻¹)	Spatial CV	Skewness	Sill	Range
Raw data	0	[0 -50]	7.32	35%	- 0.70	1889	8455
Global filtering	-13%	[1.5 – 17.2]	7.78	21%	-0.57	2.49	361
Global + local filtering	-19%	[1.5 – 17.2]	7.86	19%	-0.49	2.28	77

Satellite data collection

Remote sensing data from the Multi-Spectral Instrument (MSI) mounted on Sentinel-2 satellites were used in this study. Satellite images were downloaded from the internet platform of the French scientific structure “Theia” (*Pôle Theia, 2022*) with Python software. Acquired images correspond to level “2A” treatment also known as Bottom of Atmosphere” (BoA). Images are thus orthorectified, georeferenced by tile (100 km x 100 km) and benefit from atmosphere correction. Only wavelength with resolutions of 10m and 20m were downloaded. Acquisition period was set between the 1st of April to 30th of June from 2016 to 2021 to match wheat growing period. Revisit time is approximately five days but only images with less than 70% of cloud coverage were selected to ensure maximal availability of pixels during the season. Number of downloaded images are indicated per year and month in Table 3.

Table 3: Number of downloaded Sentinel-2 images per year and month

Year	April	May	June
2016	1	2	2
2017	2	3	1
2018	2	3	2
2019	4	2	2
2020	7	11	4
2021	4	2	8

Vegetation indices

Vegetation indices (Table 4) were calculated on the whole Sentinel-2 tiles at each sensing date available (Table 3). Each map of vegetation index was then cropped to each field boundary.

Vegetation indices were tested for their ability to reveal within-field yield variability. Red and Near Infra-Red (NIR) wavelengths respectively catch the intensity of the photosynthetic activity and the complexity of cells structure in plant leaves (Ollinger, 2011). Combining these two wavelengths, NDVI, the Normalized Difference Vegetation Index, reflects plant vigor and thus biomass development (Tucker 1979). However, NDVI is known to saturate for large Leaf Area Index (LAI) and thus high level of biomass (Haboudane et al., 2004). Considering the above-mentioned sensing period, other indices have also been tested. Modified Simple Ratio (MSR) was developed to overcome NDVI limitations in high biomass (Chen 1996, Haboudane, 2004). Enhanced Vegetation Index 2 (EVI2) is also known to perform better in high level of biomass (Huete et al. 1997, Jiang et al. 2008). Haboudane et al. (2004) transformed three-wavelengths based indices firstly dedicated to photosynthetic activity detection, Modified Chlorophyll Absorption in Reflectance Index (MCARI), into LAI sensitive indices. Modified Chlorophyll Absorption Ratio Index 1 and 2 (MCARI1, MCARI2) and Modified Triangular Vegetation Index 2 (MTVI2). Finally, two indices were calculated to ensure any disturbance of soil background, the Soil Adjusted Vegetation Index (SAVI) (Huete 1988) and the Optimized Soil Adjusted Vegetation Index (OSAVI) developed by Rondeaux et al. (1996).

Table 4: Equations of the vegetation indices used in this study

Index	Equations	Source
NDVI	$(\text{NIR} - \text{Red})/(\text{NIR} + \text{Red})$	Tucker 1979
SAVI	$1.428 \times (\text{NIR} - \text{Red})/(\text{NIR} + \text{Red} + 0.428)$	Huete 1988
OSAVI	$(1 + 0.16) \times (\text{NIR} - \text{Red})/(\text{NIR} + \text{Red} + 0.16)$	Rondeaux et al. 1996
MSR	$(\text{NIR} - \text{Blue})/(\text{Red} - \text{Blue})$	Chen 1996 Sims & Gamon 2002
EVI2	$2.5 \times (\text{NIR} - \text{Red})/(\text{NIR} + 2.4 \times \text{Red} + 1)$	Jiang et al. 2008
MCARI	$(\text{Red}_{\text{edge}} - \text{Red}) - 0.2 \times (\text{Red}_{\text{edge}} - \text{Green}) \times \left(\frac{\text{Red}_{\text{edge}}}{\text{Red}} \right)$	Daughtry et al. 2000
MCARI1	$1.2 \times (2.5 \times (\text{NIR} - \text{Red}) - 1.3 \times (\text{NIR} - \text{Green}))$	Haboudane et al. 2004
MCARI2	$1.5 \times 2.5(\text{NIR} - \text{Red}) - 1.3(\text{NIR} - \text{Green}) / \sqrt{(2\text{NIR} + 1)^2 - (6\text{NIR} - 5\sqrt{\text{Red}}) - 0.5}$	Haboudane et al. 2004
MTVI2	$1.5 \times 1.2(\text{NIR} - \text{Red}) - 1.3(\text{NIR} - \text{Green}) / \sqrt{(2\text{NIR} + 1)^2 - (6\text{NIR} - 5\sqrt{\text{Red}}) - 0.5}$	Haboudane et al. 2004

Delineation of management zones

Algorithm developed by Blackmore (2000) on yield maps follows two main steps. The first creates a spatial trend map expressing each pixel as the average of the standardized yields (1) over the years (2).

$$s_i = \left(\frac{y_i}{\bar{y}} \right) \times 100 \quad (1)$$

$$\bar{s}_i = \frac{\sum_{t=1}^n s_{it}}{n} \quad (2)$$

Where s_i is the standardized yield (y) on location i , \bar{y} is the annual yield of the field, \bar{s}_i the average of standardized yield over n years.

The second expresses the magnitude of yield variation by pixel computing the coefficient of variation (CV) (3) and creating a temporal trend map.

$$CV_i = \frac{\left(\frac{\sum_{t=1}^n s_{it}^2 - (\sum_{t=1}^n s_{it})^2}{n(n-1)} \right)^{0.5}}{\bar{s}_i} \times 100 \quad (3)$$

Values of the two generated maps are opposed to thresholds to delineate High and Stable (HS), Low and Stable (LS) and unstable (U) management zones. Blackmore algorithm requires at least three years of yield map records to be implemented.

Statistical analysis

Analysis is performed with R software (version 4.0.5) and QGIS (version 3.22).

- a. Step 1: Correlation analysis between yield and vegetation indices distributions

Yield substitution in Blackmore's method (subsection 2.5) could be performed by different vegetation indices (subsection 2.4).

The first step of the statistical analysis aims to analyze the ability of different vegetation indices to retrieve annual yield distribution at the sub-field scale. In Blackmore's approach, the first step rescales individual yield map values on the annual mean yield value (equation 1). Thus, chosen vegetation index must retrieve yield variability but doesn't have to predict yield values. To evaluate and compare VIs, we used Spearman rank correlation. This method let compare distribution ranks and stay robust with non-normal distributions. Analysis is performed on the different yield maps and vegetation indices computed from each individual satellite images sensed in related growing

periods. Once the best index is identified, we looked for sensing window offering the best and most constant correlations. Satellites images were obtained between April 1 and June 30 to match wheat growing period. Flowering stage, in our context is reached at the beginning of June (Gobin, 2018) so senescence is expected by the end of the month.

From the results obtained during these two substeps, Blackmore's method is implemented with a vegetation index; the most correlated to yield distribution and sensed during optimal window.

b. Step 2: Management zone comparison from yield maps and vegetation index

Among the fields where yield maps were obtained, six have at least three years of records. Blackmore's delineation was implemented on the yield maps and the corresponding maps of vegetation index. A confusion matrix is constructed for each field between both delineations from the yield maps (considered as the "true classes") and maps of VI (considered as the "predicted classes"). Delineated maps are compared pixels by pixels. Different metrics are computed to evaluate the accuracy of the satellite-based delineation (Makowski et al. 2009). Accuracy metrics indicates the number of well classified pixels (pixels representing management zones) among well classified and wrongly classified pixels. Sensitivity represents the rate of well classified pixels (true positives) among the total pixels classified in the same class (true positive and false positive). It can be considered as the ability of NDVI delineation to detect the correct management zone. Specificity measures the rate of pixels correctly classified in a different class (true negative) among all the pixels classified in different classes (true negative and false negative) (Tharwat, 2021). Specificity measures the exactness of the classification. Here classes are equivalent to management zones.

Results and Discussion

Identification of the best vegetation index to retrieve yield distribution

Fig 2 represents the distributions of the Spearman correlations calculated on 40 fields, including different yield maps and the related VI maps computed at each sensing dates along the related seasons. Obtained correlations strongly depend on the year of observation.

NDVI, OSAVI, SAVI, MSR and EVI2 obtained the same correlations by year. These different VI involve different combinations of the same wavelengths in the NIR and Red. OSAVI and SAVI were expected to detect potential soil disturbances at the beginning or the end of the season. However, at this sensing period, canopy is already closed, and these indices don't provide more information than NDVI. MSR and EVI2 were computed for their ability to outreach saturation issue in high biomass level. However, these results on rank correlation reveal similar performances as the one obtained with NDVI.

At the opposite, the different versions of MCARI and the MTVI2 obtained more variable results. MCARI always underperform compared to the different VIs. This index involves "red-edge" wavelength and green one but does not rely on NIR, losing scattering effect on plant cells (Ollinger 2011). MCARI is known to be linked to LAI but also to chlorophyll content variations (Haboudane 2004). Chlorophyll variations could explain noise in the signal to retrieve yield. MCARI is computed on 20m resolution when all other VIs were calculated on 10m resolution. It could have dissolved a part of the information, reducing the correlation. This last effect is expected to be limited. MCARI1, MCARI2 and MTVI2 were designed to be closer to LAI values than MCARI (*ibid*). The correlation to yield is slightly higher than

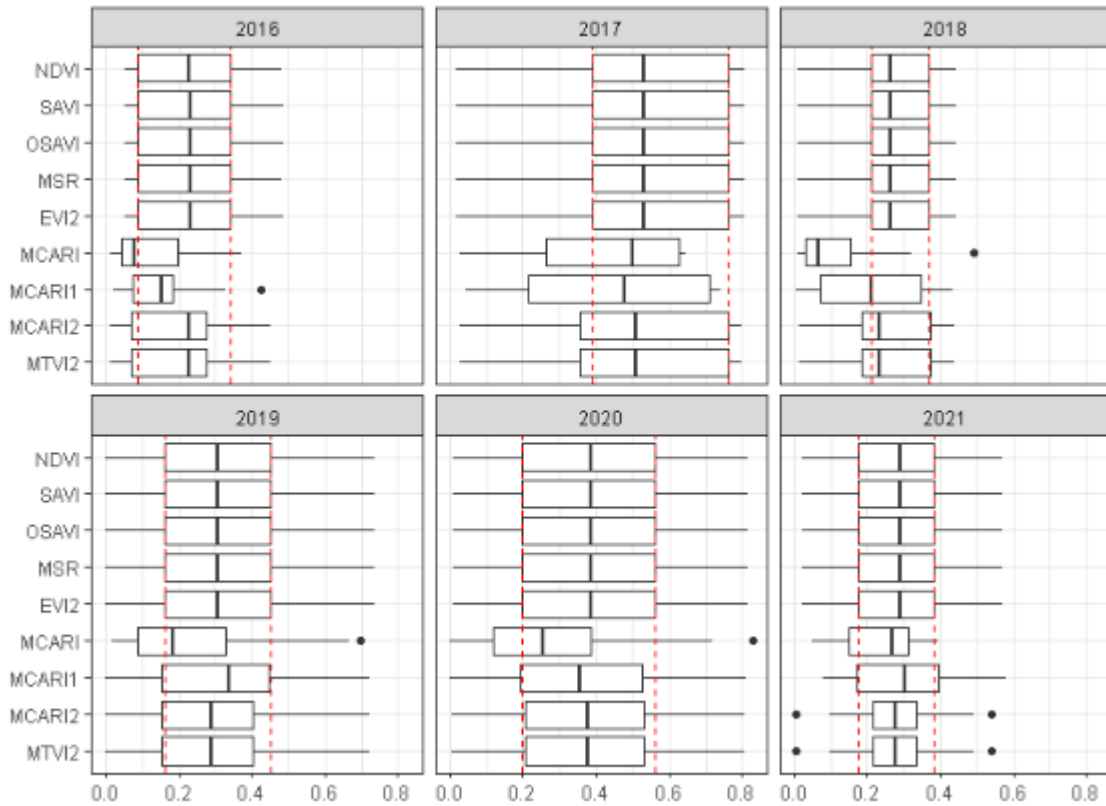


Figure 1: Distribution of Spearman rank correlation between each of the 35 fields annual yield maps and maps of vegetation indices computed at each available sensing date. The red dotted lines represent the first and third quartile of NDVI based correlation.

MCARI, irrespective of year, site and sensing date. However, these three indices didn't reach performances of "NIR-Red" indices like NDVI to retrieve yield spatial variability. Adding wavelength in the "green" domain seems to reduce the ability of the index to catch yield variability.

Correlation levels obtained with NDVI are consistent with correlations observed in the literature to analyze annual within-field yield spatial patterns on the same growing periods (Maestrini et Basso, 2018; Toscano et al. 2019). Most articles use « Pearson » correlation as the objective is to regress yield through NDVI values.

From these results, no index better perform than NDVI to catch spatial yield variability within the fields. This index is the main used in closed-related literature (Lai et al. 2018; Basso et al. 2019; Toscano et al. 2019) and can be computed on high spatial resolution (10m) from Sentinel-2 images. For these reasons, NDVI is the index selected in this study as a proxy of within-field spatial variations.

Identification of the best sensing window

In the next sections, only NDVI will be used to retrieve yield variations. Fig 3. represent distributions of Spearman correlations computed between yield and NDVI for different fields, year and available sensing dates along the growing period. Correlations are grouped per week as this time resolution corresponds approximately to the revisit time of Sentinel-2 missions.

The year 2016 was removed from the graph as many pixels were missing from the different satellite images.

Correlation levels change from year to year with globally higher correlation in 2017 than in other years. A trend is observed among fields and years to reach higher correlations at the end of May and beginning of June. This trend seems to move within a three weeks period from May 15th

(2019) to June 7th (2018, 2020). This period corresponds to the wheat flowering stage in Belgian context (Gobin, 2018) when wheat leaves are already totally developed and not yet senescent. In 2021, correlations seem the highest in the end of April. Even if a limited tendency is also observed in 2017 and 2018 these higher correlations seem more anecdotal than the window observed in May-June.

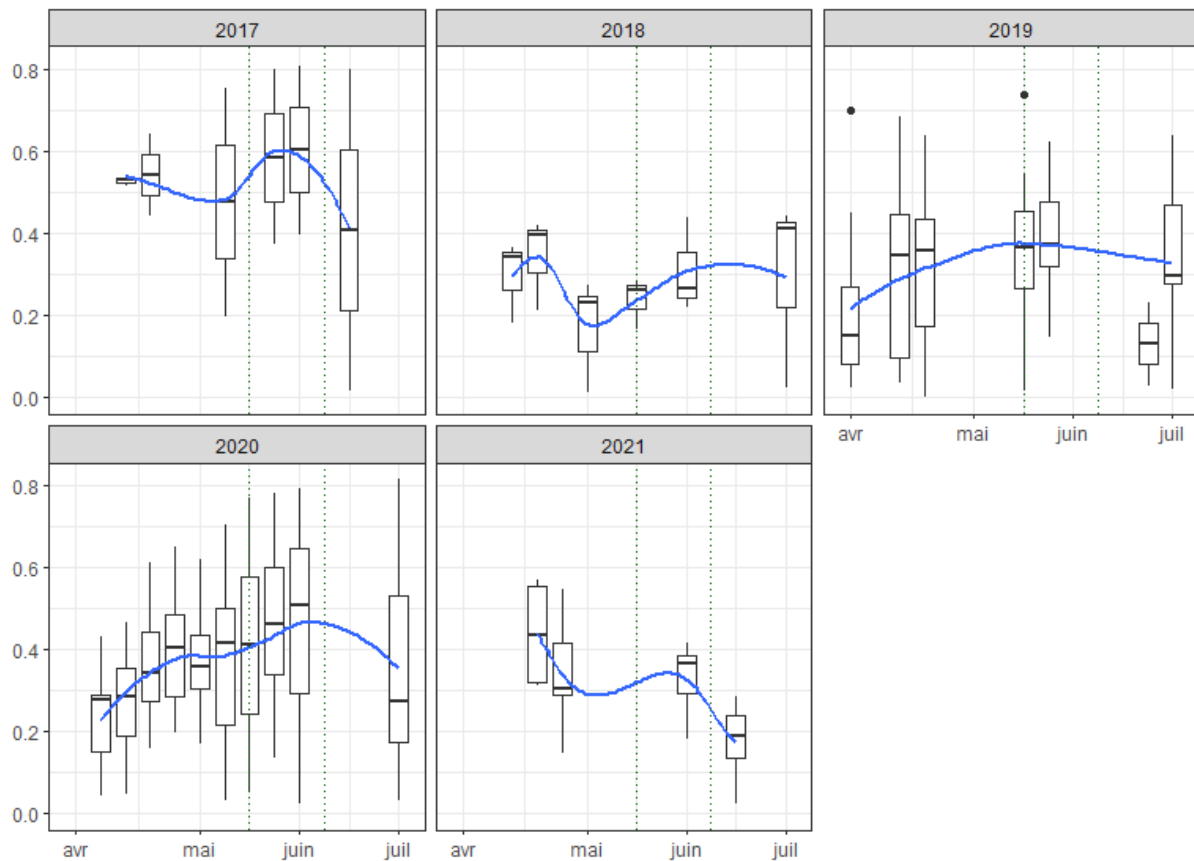
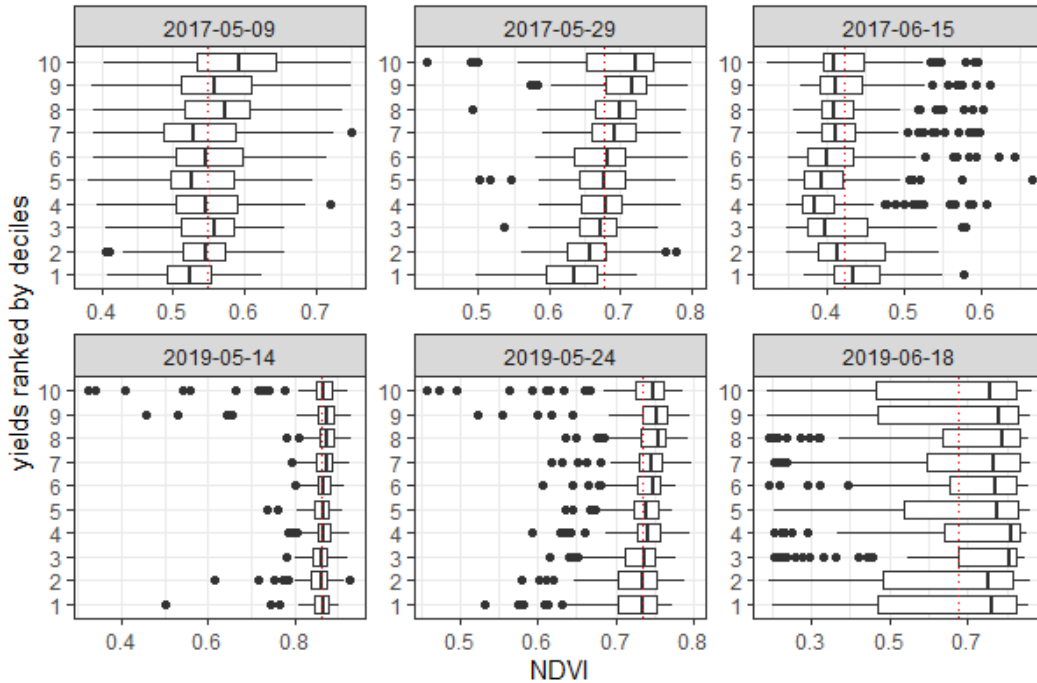


Figure 2: Spearman correlation distributions computed between yield maps and NDVI on related sensing dates over the growing period. Correlations are grouped per week Vertical dotted lines define the three weeks period between May 15th and June 7th.

Our results are consistent with ones obtained by Panek et al 2020 whose correlations are also the highest during flowering stage. Correlations we computed are globally weaker but based on yield maps rather than plant sampling. The remaining heterogeneity of yield maps after outlier removal (Table 2) could partly explain these weak correlations. We can observe on the example below a “noisy” yield map and related vegetation indices computed on one sensing date. From our results, we can expect a clearer delineation of management zones applying Blackmore’s methodology with NDVI.

However, NDVI is an index that usually range between 0 and 1 in vegetation. Correlations obtained show that the entirety of yield distribution is not clearly caught by NDVI (Figure 2). Figure 4 displays the distributions of NDVI within yield classes, ranked per yield deciles, at different dates from the same year and on one field. Among the different dates, “2017-05-29” got the best correlation. At this date, NDVI is also visually more discriminant of the yield classes.

Figure 4: NDVI distributions by yields ranked per yield deciles, on different dates and one field. Red dotted lines represent NDVI mean values per date.



As Spearman correlation compares yield and NDVI ranks, low correlation indicates a low ability of the index to retrieve yield distribution. This could affect Blackmore’s delineation accuracy and requires a validation of the delineation.

Comparison of Blackmore’s delineation from yield maps and maps of NDVI

Table 5 summarizes the metrics computed from the confusion matrix between yield map-based delineation and NDVI-based delineation.

Table 5: Metrics of management zones classification accuracy computed on each field F1 to 6.

Fields	Accuracy	Sensitivity			Specificity		
		HS	LS	U	HS	LS	U
F1	0.625	0.777	0.484	0.000	0.502	0.768	0.994
F2	0.599	0.661	0.567	0.000	0.571	0.648	0.998
F3	0.731	0.855	0.681	0.000	0.673	0.816	0.995
F4	0.754	0.776	0.748	0.000	0.746	0.773	0.996
F5	0.436	0.250	0.701	0.000	0.806	0.277	0.937
F6	0.632	0.829	0.448	0.000	0.464	0.846	0.983
Average	0.630	0.691	0.605	0.000	0.627	0.688	0.984

Accuracy of the delineation ranges between 0.43 and 0.75 highlighting important differences in classifications. Sensitivity of U zones reveals the misfit of Blackmore’s stability threshold to NDVI. However, few U zones were originally detected by yield map based delineation, explaining the high specificity of this zone. High and stable zones got the best predictions (sensitivity), except on the field F5 (sensitivity=0.25) which also obtained the lowest accuracy. LS zones were globally less predicted than HS indicating a transfer of LS and U pixels toward HS. Indeed, LS got higher

values of specificity than HS. This offset between HS and LS predictions can be explained by the shapes of yield and NDVI distributions (figures 5 and 6). Indeed, in Blackmore’s method, annual yield records are compared to annual mean yield. This mean threshold separates the higher yields from the lower yields. When using the NDVI, the mean value seems not to be a good threshold to distinguish high and low NDVI values related to the yield level (figure 6).

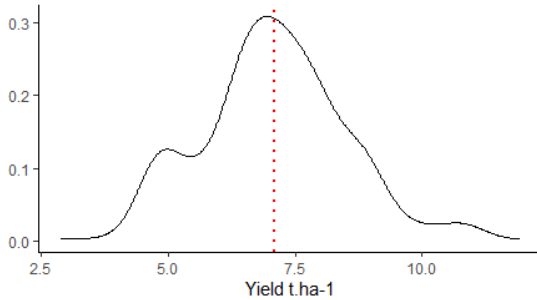


Figure 5: Shape of annual within-field yield distribution.
Red dotted line is the mean yield value

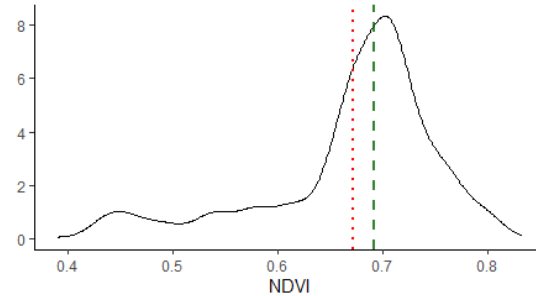


Figure 6: Shape of annual within-field NDVI distribution. Red dotted line is the mean NDVI value and green dashed line is the median NDVI

A first approach incrementally adapts NDVI threshold on each map of NDVI from the annual mean NDVI. Threshold range from -0.5 to 0.5, “0” being the mean value. Accuracy is computed on confidence matrix between yield map-based delineation and NDVI based delineation for the different values of NDVI threshold. Results are shown on figure 7. Optimal accuracy is reached from different thresholds according to the field considered. As an example, mean NDVI seems to be the optimal threshold for field F4 whereas “mean NDVI + 0.05” is the optimal threshold for field F5. Usually, mean is considered a poor indicator for non-normal distribution; the median is rather used. Same computation is applied replacing the mean by the median of NDVI (figure 8). Initial NDVI median seems a better threshold than mean NDVI as optimal accuracy values on the different fields are centered on the median (figure 7 & 8).

Finally, the different confusion matrix indices are computed implementing NDVI median as threshold to separate values of NDVI corresponding to higher yields from those considered as lower yields (table 6).

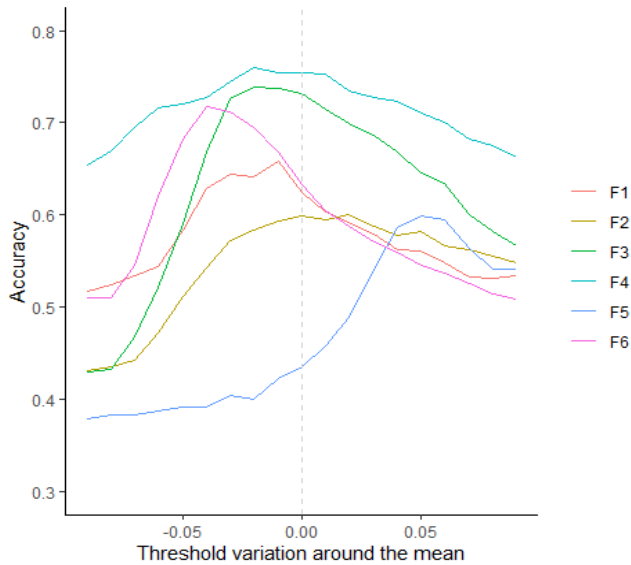


Figure 7: Accuracy values from confusion matrices computed between yield map-based management zones and NDVI-based management zones when NDVI threshold evolve around the mean. F1 to F6 are the six fields where the delineation is computed.

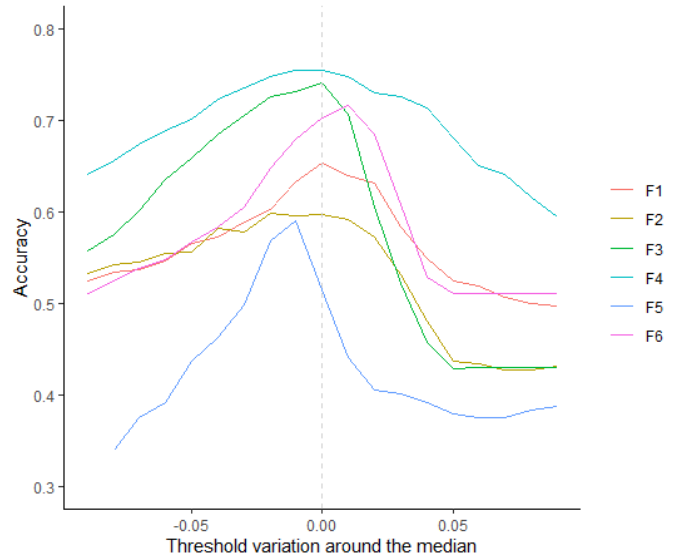


Figure 8: Accuracy values from confusion matrices computed between yield map-based management zones and NDVI-based management zones when NDVI threshold evolve around the median. F1 to F6 are the six fields where the delineation is computed.

Table 1: Metrics of management zones classification accuracy computed on each field F1 to 6

Fields	Accuracy	Sensitivity			Specificity		
		HS	LS	U	HS	LS	U
F1	0.654	0.723	0.596	0.000	0.599	0.714	1.000
F2	0.597	0.636	0.594	0.000	0.599	0.624	0.997
F3	0.742	0.742	0.841	0.000	0.826	0.702	0.996
F4	0.754	0.738	0.789	0.000	0.790	0.733	0.996
F5	0.515	0.508	0.557	0.000	0.728	0.562	0.887
F6	0.702	0.684	0.722	0.000	0.731	0.697	0.989
Average	0.661	0.672	0.683	0.000	0.712	0.672	0.978

Accuracy of the prediction slightly improved on the different fields. Sensitivity of LS increased more than HS, which was expected. Both classes reached equivalent sensitivity values. At the same time, the specificity of HS increased while LS decreased indicating that HS are still better predicted than LS. U zones that did represent a low part of the delineated pixels are not better predict. Further investigations are needed to adapt threshold of NDVI temporal variations. Figures 9 and 10 give an overview of delineation of field F2

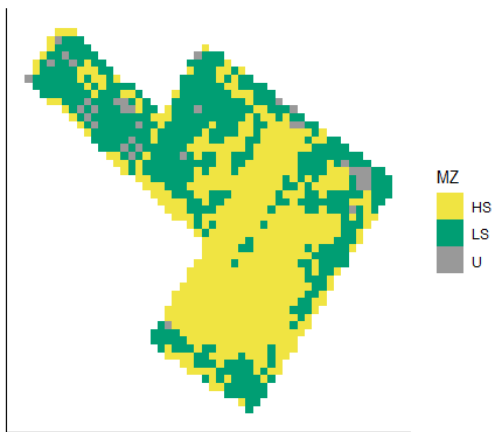


Figure 9: Yield map- based delineation on field F2

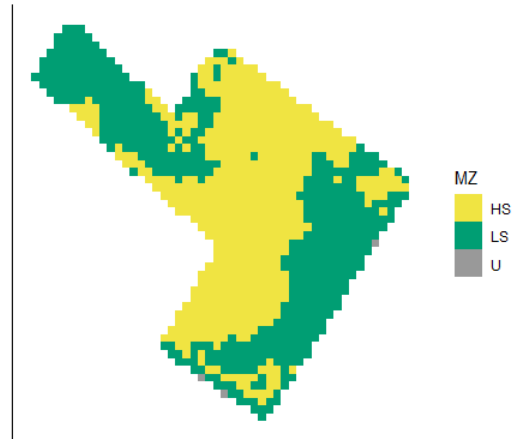


Figure 10: NDVI-based delineation on field F2

Conclusion

Diagnosis of within-field variability already offers a wide field of research as it would be a powerful support to reduce agricultural pollutions while improving productions quantity and quality. In Western-Europe, statement of technology adoption raises the issue of the future of precision agriculture. We assumed a low-tech approach would favor appropriation of new agronomic techniques by farmers. Replacement of yield maps by vegetation indices in delineation methods would level up the scale of application of such diagnosis. We have shown that NDVI is still an interesting index, applied at the canopy level, to retrieve yield variations. Implementing NDVI into Blackmore's delineation method is promising but needs further adaptations to correctly catch the within-field spatial and temporal trends. Special attention was paid to distinguish low from high yielding zones as unstable zones were reduced in our dataset. However, the inability of the index to catch temporal trend negatively affect the global accuracy of NDVI-based delineation. This calibration will support deployment of the method at the territorial level on both Hauts-de-France and Wallonia regions. This diagnosis will benefit farmers who want to adapt their N management practices at the subfield scale. Moreover, this territorial delineation, coupled with a crop model, will support further investigations to implement decision rules adapted to the different management zones.

Acknowledgements

This study was possible thanks to different farmers and an organization. We thank Mr Rivenet, Mr Goffaux and the "Ferme 3.0" to share with us their yield maps. This study was made possible thanks to the support of the Research Commission of the Catholic University of Lille and the support of the University of Liege.

References

- Agreste 2020. Memento 2020 – Hauts-de-France. Agreste, La statistique, l'évaluation et la prospective agricole.
- Ahamed T., Tian L., Zhang Y., & Ting K.C., 2011. A review of remote sensing methods for biomass feedstock production, *Biomass and Bioenergy*, Volume 35, Issue 7, Pages 2455-2469. <https://doi.org/10.1016/j.biombioe.2011.02.028>.
- Ambler B. & Smith M-P., 1991. Sensing and mapping grain yield variations. In: *Proceedings ASAE Symposium on Automated Agriculture for the 21st Century*, 16-17 Dec. 1991, Chicago, Ill. American Society of Agricultural Engineers, St Joseph, Mich., pp. 35-364.
- Barnes, A., Soto, I.D., Eory, V., Beck, B., Balafoutis, A., Sánchez, B., Vangeyte, J., Fountas, S., 2019. agricultural technologies within arable farming systems 10.
- Basso, B., Bertocco M., Sartori, L., Martin, E.C., 2007. Analyzing the effects of climate variability on spatial pattern of yield in

- a maize–wheat–soybean rotation. *European Journal of Agronomy* 26, 82–91. <https://doi.org/10.1016/j.eja.2006.08.008>
- Basso, B., Ritchie, J.T., Cammarano, D., Sartori, L., 2011. A strategic and tactical management approach to select optimal N fertilizer rates for wheat in a spatially variable field. *European Journal of Agronomy* 35, 215–222. <https://doi.org/10.1016/j.eja.2011.06.004>
- Basso, B., Shuai, G., Zhang, J., Robertson, G.P., 2019. Yield stability analysis reveals sources of large-scale nitrogen loss from the US Midwest. *Sci Rep* 9, 5774. <https://doi.org/10.1038/s41598-019-42271-1>
- Blackmore, S., 2000. The interpretation of trends from multiple yield maps. *Computers and Electronics in Agriculture* 26, 37–51. [https://doi.org/10.1016/S0168-1699\(99\)00075-7](https://doi.org/10.1016/S0168-1699(99)00075-7)
- Billen, G., Garnier J, Benoît, M, Anglade J, 2013. La cascade de l'azote dans les territoires de grande culture du Nord de la France. *Cah Agric* 22: 272-81. doi :10.1684/agr.2013. (<https://revues.cirad.fr/index.php/cahiers-agricultures/article/view/31032/30792>)
- Birrell, S.J., Sudduth, K.A., Borgelt, S.C., 1996. Comparison of sensors and techniques for crop yield mapping. *Computers and Electronics in Agriculture, Spatially Variable Field Operations* 14, 215–233. [https://doi.org/10.1016/0168-1699\(95\)00049-6](https://doi.org/10.1016/0168-1699(95)00049-6)
- Bonjean, A-C., Fangeat E, Forget, A., Fustec, A., Habe, C., Jaeger, R., Moiroud, L., Morales, E., Chabot, C., (2022). État des lieux et perspectives des démarches « low-tech ». Rapport - 52 pages
- Cassman, K.G., Dobermann, A., 2022. Nitrogen and the future of agriculture: 20 years on. *Ambio* 51, 17–24. <https://doi.org/10.1007/s13280-021-01526-w>
- Chen J.M. 1996. Evaluation of vegetation indices and a Modified Simple Ratio for boreal applications. *Canadian Journal of Remote Sensing*. 22: 229-242.
- Daughtry C.S.T, Walthall C.L., Kim M.S., Brown de Colstoun E. and McMurtrey E. (2000). Estimating corn leaf chlorophyll concentration from leaf and canopy reflectance. *Remote Sensing of Environment*. 74: 229-239.
- Delloye, C., Weiss, M., Defourny, P., 2018. Retrieval of the canopy chlorophyll content from Sentinel-2 spectral bands to estimate nitrogen uptake in intensive winter wheat cropping systems. *Remote Sensing of Environment* 216, 245–261. <https://doi.org/10.1016/j.rse.2018.06.037>
- Dumont, B., Basso, B., Bodson, B., Destain, J.-P., Destain, M.-F., 2015. Climatic risk assessment to improve nitrogen fertilisation recommendations: A strategic crop model-based approach. *European Journal of Agronomy* 65, 10–17. <https://doi.org/10.1016/j.eja.2015.01.003>
- ESA, 2015. Sentinel-2 User Handbook. *European Spatial Agency – European Commission*. p 36.
- Fang, H., Baret, F., Plummer, S., & Schaepman-Strub, G. (2019). An overview of global leaf area index (LAI): Methods, products, validation, and applications. *Reviews of Geophysics*, 57, 739-799. <https://doi.org/10.1029/2018RG000608>
- Filippi, P. et al. An approach to forecast grain crop yield using multi-layered, multi-farm data sets and machine learning. *Precision Agric* 20, 1015–1029 (2019).
- Fowler D et al. 2013. The global nitrogen cycle in the twenty first century. *Phil Trans R Soc B* 368 : 20130164. <http://dx.doi.org/10.1098/rstb.2013.0164>
- Franch, B. et al. Remote sensing-based yield monitoring: Application to winter wheat in United States and Ukraine. *International Journal of Applied Earth Observation and Geoinformation* 76, 112–127 (2019).
- Galloway, J.N., Aber, J.D., Erisman, J.W., Seitzinger, S.P., Howarth, R.W., Cowling, E.B., Cosby, B.J., 2003. The Nitrogen Cascade. *BioScience* 53, 341. [https://doi.org/10.1641/0006-3568\(2003\)053\[0341:TNC\]2.0.CO;2](https://doi.org/10.1641/0006-3568(2003)053[0341:TNC]2.0.CO;2)
- GIS Sol 2019. Les sols dominants de France métropolitaine. Groupement d'intérêt scientifique sur les sols et Réseau Mixte Technologique Sols & Territoires, Pédologie.
- Gobin, A., 2018. Weather related risks in Belgian arable agriculture. *Agricultural Systems* 159, 225–236. <https://doi.org/10.1016/j.agsy.2017.06.009>
- Haboudane, D., 2004. Hyperspectral vegetation indices and novel algorithms for predicting green LAI of crop canopies: Modeling and validation in the context of precision agriculture. *Remote Sensing of Environment* 90, 337–352. <https://doi.org/10.1016/j.rse.2003.12.013>
- Hawkesford, M.J., Riche, A.B., 2020. Impacts of G x E x M on Nitrogen Use Efficiency in Wheat and Future Prospects. *Frontiers in Plant Science* 11.
- Huete A., Didan K., van Leeuwen W., Miura T., Glenn E. Land Remote Sensing and Global Environmental Change: NASA's Earth Observing System and the Science of ASTER and MODIS. 2008. MODIS Vegetation Indices.
- IRM (Institut Royal de Météorologie), 2021. Bilans climatologiques de 2021 [WWW Document]. URL <https://www.meteo.be/en/weather/observations/belgium>
- Jiang, Z., Huete, A. R., Didan, K., & Miura, T. (2008). Development of a two-band enhanced vegetation index without a blue band. *Remote sensing of Environment*, 112(10), 3833-3845.
- Khosla, R., D. G. Westfall, R. M. Reich, J. S. Mahal, and W. J. Gangloff. 2010. Spatial variation and site-specific management zones. In: M. A. Oliver (ed.), *Geostatistical Applications for Precision Agriculture*. Springer, Dordrecht, Netherlands
- Lachia N, Pichon L, Marcq P., Taylor J.-A. and Tisseyre B., 2021. Why are yield sensors seldom used by farmers? A French case study. Conference: 13th European Conference on Precision Agriculture.
- Lai, Y. R. et al. An empirical model for prediction of wheat yield, using time-integrated Landsat NDVI. *International Journal of Applied Earth Observation and Geoinformation* 72, 99–108 (2018).

- Le Bas C., 2021, "Carte de la profondeur du sol issue de la Base de Données Géographique des Sols de France", <https://doi.org/10.15454/7ZDND6>, Portail Data INRAE, V1
- Lécuyer, B., Chatellier, V., Daniel, K., 2014. Analysis of price volatility of mineral fertilisers: possible issues for European farmers. *International Journal of Agricultural Resources, Governance and Ecology* 10, 344–361. <https://doi.org/10.1504/IJARGE.2014.066255>
- Legrain, X., & Bock, L. (2009). Légende de la Carte Numérique des Sols de Wallonie-Tableau simplifié.
- Lemaire, G., Jeuffroy, M.-H., Gastal, F., 2008. Diagnosis tool for plant and crop N status in vegetative stage. *European Journal of Agronomy* 28, 614–624. <https://doi.org/10.1016/j.eja.2008.01.005>
- Leroux, C., Jones, H., Clenet, A., Dreux, B., Becu, M., Tisseyre, B., (2018). A general method to filter out defective spatial observations from yield mapping datasets. *Precision Agric* 19, 789–808. <https://doi.org/10.1007/s11119-017-9555-0>
- Leroux C. (2020). R codes to be used within QGIS for Precision Agriculture applications. https://github.com/Corentin39-aspeixit/R-QGIS-Precision-Agriculture/blob/master/R_codes/ [Accessed December 2021]
- Lyle, G., Bryan, B.A., Ostendorf, B., 2014. Post-processing methods to eliminate erroneous grain yield measurements: review and directions for future development. *Precision Agric* 15, 377–402. <https://doi.org/10.1007/s11119-013-9336-3>
- Maestrini, B., Basso, B., 2018. Predicting spatial patterns of within-field crop yield variability. *Field Crops Research* 219, 106–112. <https://doi.org/10.1016/j.fcr.2018.01.028>
- Makowski, D., Tichit, M., Guichard, L., Van Keulen, H., Beaudoin, N., 2009. Measuring the accuracy of agro-environmental indicators. *Journal of Environmental Management* 90, S139–S146. <https://doi.org/10.1016/j.jenvman.2008.11.023>
- Marti, J., J. Bort, G.a. Slafer, et J.I. Araus. « Can Wheat Yield Be Assessed by Early Measurements of Normalized Difference Vegetation Index? » *Annals of Applied Biology* 150, n° 2 (2007): 253-57. <https://doi.org/10.1111/j.1744-7348.2007.00126.x>.
- Meynard, J.-M., Justes, E., Machet, J.-M., Recous, S., 1997. Fertilisation azotée des cultures annuelles de plein champs. In: INRA (ed) *Maitrise de l'azote dans les agrosystèmes*, Les colloques, Reims, 183–200.
- Mulla, David, et Raj Khosla. « Historical Evolution and Recent Advances in Precision Farming ». In *Soil-Specific Farming*, édité par Rattan Lal et B Stewart, 1-36. CRC Press, 2015. <https://doi.org/10.1201/b18759-2>.
- Nysten A., Van der Verren B., Blanchard R., Vandenberghe C., Legrand J., Stalport A., Mahieu O., Abras M., Heens B., Godden B., Pierreux J., Reuter V., Blondiau L.-M., Collin C., Vilet A., Godin B., Van Remoortel V. & Dumont B., 2022. La fertilisation azotée. Itinéraire technique des céréales d'hiver. In: « Dumont B. & Henriët F. 2022. Livre Blanc Céréales – Edition Février 2022 »
- Ollinger S.V., 2011. Sources of variability in canopy reflectance and the convergent properties of plants. *New Phytologist* 189: 375–394. doi: 10.1111/j.1469-8137.2010.03536.x
- Panek, E., Gozdowski, D., Stępień, M., Samborski, S., Ruciński, D. and Buszke, B., 2020. Within-field relationships between satellite-derived vegetation indices, grain yield and spike number of winter wheat and triticale. *Agronomy*, 10(11), p.1842.
- Pierpaoli, E., Carli, G., Pignatti, E., Canavari, M., 2013. Drivers of Precision Agriculture Technologies Adoption: A Literature Review. *Procedia Technology* 8, 61–69. <https://doi.org/10.1016/j.protcy.2013.11.010>
- Pôle Theia, 2022. Value-Adding Products and Algorithms for Land Surfaces. Retrieved from <https://www.theia-land.fr/en/homepage-en/> [Accessed January 2022].
- Raun, W.R., Solie, J.B., Johnson, G.V., Stone, M.L., Lukina, E.V., Thomason, W.E. and Schepers, J.S., 2001. In-season prediction of potential grain yield in winter wheat using canopy reflectance. *Agronomy Journal*, 93(1), pp.131-138.
- Ravier C., Jeuffroy M-H. & Meynard J-M., (2016) Mismatch between a science-based decision tool and its use: The case of the balance-sheet method for nitrogen fertilization in France, *NJAS: Wageningen Journal of Life Sciences*, 79:1, 31-40, DOI: 10.1016/j.njas.2016.10.001
- Revill, A., Florence, A., MacArthur, A., Hoad, S.P., Rees, R.M., Williams, M., 2019. The Value of Sentinel-2 Spectral Bands for the Assessment of Winter Wheat Growth and Development. *Remote Sensing* 11, 2050. <https://doi.org/10.3390/rs11172050>
- Rondeaux G., Steven M. & Baret F. (1996) Optimization of soil-adjusted vegetation indices. *Remote Sensing of Environment*. 55: 97-107.
- Rose, D.C., Chilvers, J., 2018. Agriculture 4.0: Broadening Responsible Innovation in an Era of Smart Farming. *Frontiers in Sustainable Food Systems* 2.
- Sims D.A. & Gamon J.A. (2002). Relationships between leaf pigment content and spectral reflectance across a wide range of species, leaf structures and development stages. *Remote Sensing of Environment*. 81: 337-354.
- SPW 2022. Productions Végétales. [WWW Document]. URL: <https://etat-agriculture.wallonie.be/contents/indicator sheets/EAW2.html#> [Accessed April 2022]
- Sutton, M.A., Howard, C.M., Erisman, J.W., Bleeker, A., Billen, G., Grennfelt, P., & Van Grinsven, H. Grizzetti, B., 2011. *The European Nitrogen Assessment Sources, Effects and Policy Perspectives*. United Kingdom: Cambridge University Press.
- Tharwat, A., 2021. Classification assessment methods. *Applied Computing and Informatics* 17, 168–192. <https://doi.org/10.1016/j.aci.2018.08.003>
- Toscano, P., Castrignanò, A., Di Gennaro, S.F., Vonella, A.V., Ventrella, D., Matese, A., 2019. A Precision Agriculture Approach for Durum Wheat Yield Assessment Using Remote Sensing Data and Yield Mapping. *Agronomy* 9, 437. <https://doi.org/10.3390/agronomy9080437>

Tucker, C.J., 1979. Red and photographic infrared linear combinations for monitoring vegetation. *Remote Sensing of Environment* 8, 127–150. [https://doi.org/10.1016/0034-4257\(79\)90013-0](https://doi.org/10.1016/0034-4257(79)90013-0)

Weiss, M., Jacob, F., Duveiller, G., 2020. Remote sensing for agricultural applications: A meta-review. *Remote Sensing of Environment* 236, 111402. <https://doi.org/10.1016/j.rse.2019.111402>